Supplementary Material for

On the morphology of non-spherical particles using tandem aerodynamic diameter, mobility diameter, and mass measurements

Mohsen Kazemimanesh, Md Mostafizur Rahman, Dumitru Duca, Tyler J. Johnson, Ahmed Adad, George Giannopoulos, Cristian Focsa, Adam M. Boies

S1. Uncertainty analysis

The uncertainty analysis of the reported results in the present study was conducted based on ANSI/ASME Measurement Uncertainty Standard (Abernethy et al., 1985). In calculating the total uncertainty, two types of uncertainties should be considered: (i) precision uncertainty (also known as random error) and (ii) bias uncertainty (also known as systematic or instrument error). The precision uncertainty is calculated from repeated measurements and, for a small number of samples ($n < 30$), is calculated from the following equation

$$P_x = t_{1-c,n-1}\frac{\sigma_n}{\sqrt{n}} \tag{S1}$$

where P_x is the precision uncertainty in quantity x, n is the number of samples (repeated measurements), $t_{1-c,n-1}$ is the Student's t-distribution variable at confidence interval of c (95% in this study) and degree of freedom of $n-1$, and σ_n is the standard deviation of samples (square-root of the variance).

The bias uncertainty, B_x, is the error of the instrument to read the correct value of a measurement. When a reported parameter depends on two or more independent variables as $f(x_1, x_2, x_3, \dots)$, the propagation of uncertainty is used as follows:

$$B_x = \sqrt{\left(\Delta x_1 \frac{\partial f}{\partial x_1}\right)^2 + \left(\Delta x_2 \frac{\partial f}{\partial x_2}\right)^2 + \left(\Delta x_3 \frac{\partial f}{\partial x_3}\right)^2 + \cdots} \tag{S2}$$

where Δ denotes the uncertainty in the corresponding independent variable. The total uncertainty, U_x, is then estimated as follows

$$U_x = \sqrt{P_x^2 + B_x^2} \tag{S3}$$

The instruments used for the measurement of effective density had the following bias uncertainties: 3% in particle mobility diameter measurement using the DMA (Kinney et al., 1991), 2.7% in mass measurement of singly-charged particles using the CPMA (Symonds et al., 2013), and 4.3% in particle aerodynamic diameter measurement using the AAC (Tavakoli & Olfert, 2014).

To calculate the bias uncertainty in effective density using a combination of any two instruments, the principle of propagation of bias uncertainty was used. Using the DMA-CPMA method, the particle effective density is determined using the following equation as noted in Section 2 of the manuscript

$$\rho_{\text{eff}} = \frac{6m}{\pi d_{\text{m}}^3} \tag{S4}$$

and its bias uncertainty, $\Delta\rho_{\text{eff}}$, is calculated as

$$\frac{\Delta\rho_{\text{eff}}}{\rho_{\text{eff}}} = \sqrt{\left(\frac{\Delta m}{m}\right)^2 + 9\left(\frac{\Delta d_{\text{m}}}{d_{\text{m}}}\right)^2} = \sqrt{(0.027)^2 + 9(0.03)^2}\sim 9.4\% \quad \text{(S5)}$$

where Δ denotes the uncertainty (error) in the corresponding physical quantity.

Using the AAC-DMA method, the particle effective density is determined using the following equation as noted in Section 2 of the manuscript

$$\rho_{\text{eff}} = \rho_0 \frac{d_{\text{a}}^2 C_{\text{c}}(d_{\text{a}})}{d_{\text{m}}^2 C_{\text{c}}(d_{\text{m}})} \quad \text{(S6)}$$

The mean uncertainty in Cunningham slip correction factor, C_{c}, for particle diameter in the range of 20–270 nm is ~2.5% (Kim et al., 2005). Thus, the bias uncertainty in effective density is calculated as

$$\begin{aligned}\frac{\Delta\rho_{\text{eff}}}{\rho_{\text{eff}}} &= \sqrt{4\left(\frac{\Delta d_{\text{a}}}{d_{\text{a}}}\right)^2 + \left(\frac{\Delta C_{\text{c}}(d_{\text{a}})}{C_{\text{c}}(d_{\text{a}})}\right)^2 + 4\left(\frac{\Delta d_{\text{m}}}{d_{\text{m}}}\right)^2 + \left(\frac{\Delta C_{\text{c}}(d_{\text{m}})}{C_{\text{c}}(d_{\text{m}})}\right)^2} \\ &= \sqrt{4(0.043)^2 + (0.025)^2 + 4(0.03)^2 + (0.025)^2}\sim 11.1\%.\end{aligned} \quad \text{(S7)}$$

Using the AAC-CPMA method, the particle effective density is determined using the following equation as noted in Section 2 of the manuscript

$$\rho_{\text{eff}} = \left(\frac{\pi d_{\text{a}}^3}{6m}\right)^2 \left(\frac{\rho_0 C_{\text{c}}(d_{\text{a}})}{C_{\text{c}}(d_{\text{m}})}\right)^3 \quad \text{(S8)}$$

and the bias uncertainty in effective density is calculated as

$$\begin{aligned}\frac{\Delta\rho_{\text{eff}}}{\rho_{\text{eff}}} &= \sqrt{36\left(\frac{\Delta d_{\text{a}}}{d_{\text{a}}}\right)^2 + 9\left(\frac{\Delta C_{\text{c}}(d_{\text{a}})}{C_{\text{c}}(d_{\text{a}})}\right)^2 + 4\left(\frac{\Delta m}{m}\right)^2 + 9\left(\frac{\Delta C_{\text{c}}(d_{\text{m}})}{C_{\text{c}}(d_{\text{m}})}\right)^2} \\ &= \sqrt{36(0.043)^2 + 9(0.025)^2 + 4(0.027)^2 + 9(0.025)^2}\sim 28.4\%.\end{aligned} \quad \text{(S9)}$$

S2. Technical specifications of the GDI engine

The technical specifications of the GDI engine used in the present study are summarized in Table S1.

Table S1: Engine specifications (bTDC means before Top Dead Center and aTDC means after Top Dead Center)

Specification	Value
Cylinder head	Pent-roof type
Compression ratio	12.5:1
Bore	82 mm
Stroke	85 mm
Stroke volume	449 cm^3
Fuel direct injection system	Central mounted generic six-hole injector
Injection pressure	150 bars
Spark plug location	Exhaust side
Intake Valve Open	334° bTDC
Intake Valve Close	166° bTDC
Exhaust Valve Open	154° aTDC
Exhaust Valve Close	330° aTDC

S3. Raw data plots of mass spectral densities

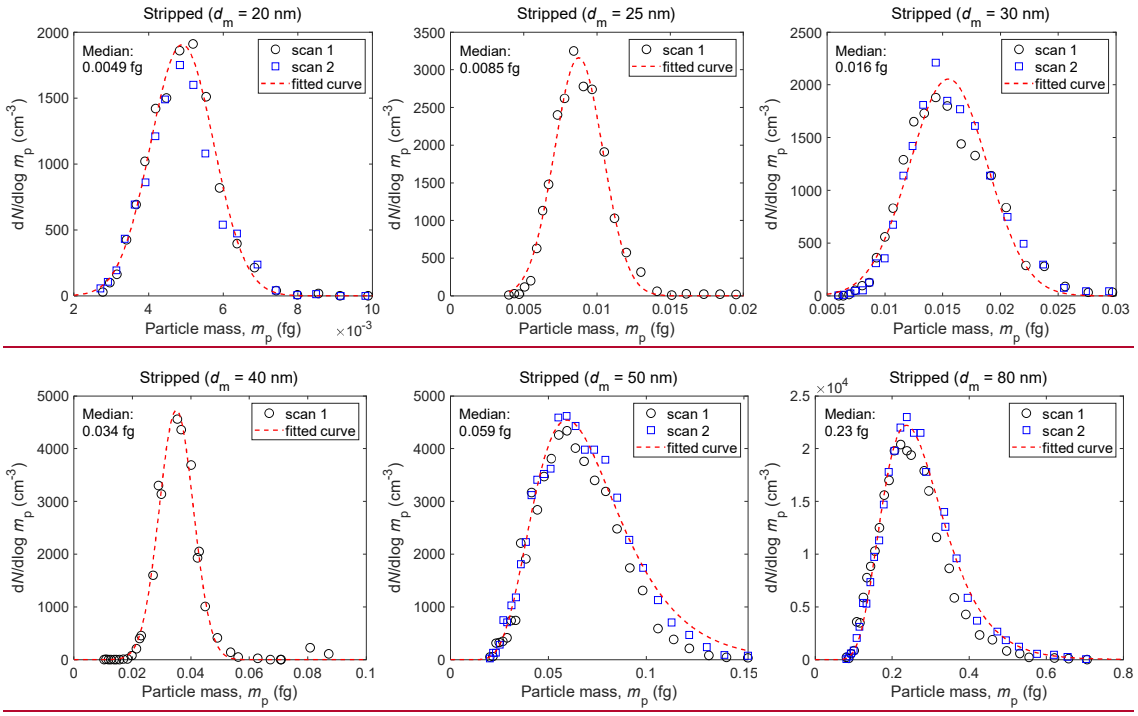

Figure S1: Mass spectral density of representative stripped particles (at engine speed of 1200 rpm and load of 6 bar). The dashed line shows the unimodal lognormal fit to the data and the median mass used in Figure 4 is shown in the top left corner of each plot.

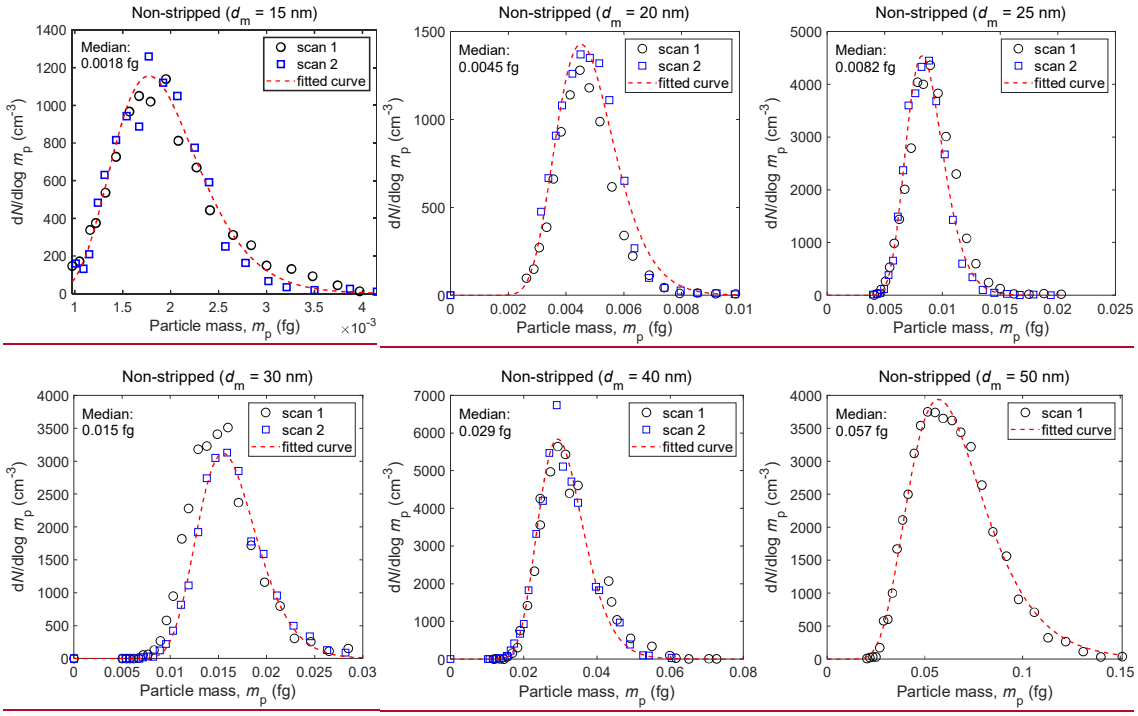

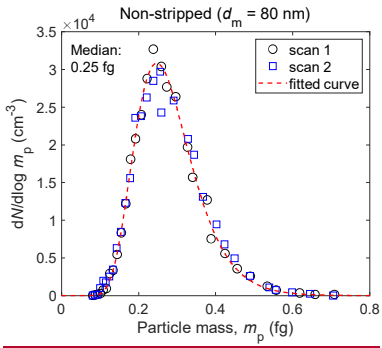

Figure S2: Mass spectral density of representative non-stripped particles (at engine speed of 1200 rpm and load of 6 bar). The dashed line shows the unimodal lognormal fit to the data and the median mass used in Figure 4 is shown in the top left corner of each plot.

S1. Penetration efficiency of the catalytic stripper

The penetration efficiency of the catalytic stripper at 350 °C has also been measured by Woo et al. (2021) and a comparison of this data with the manufacturer's penetration function is shown in Figure S3.

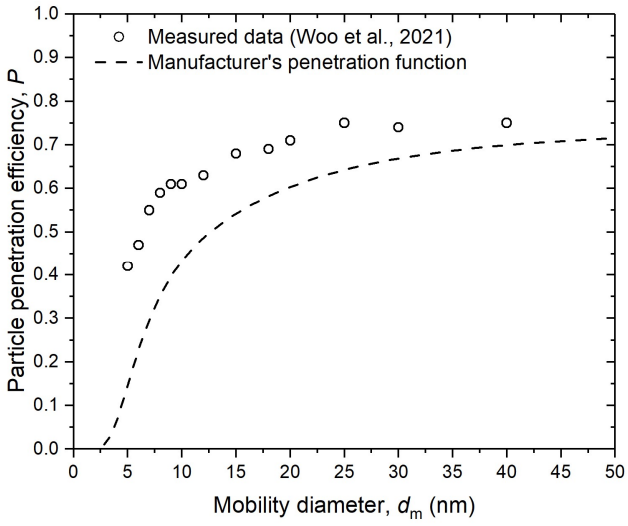

Figure S3: Penetration efficiency of the catalytic stripper at 350 °C. The data points are the measurements taken from Woo et al. (2021). The dashed line shows the penetration function supplied by the manufacturer.

~~S3.~~S4. Mass-mobility of polydisperse particles

The mass-mobility relationships and the effective density of non-stripped and stripped polydisperse particles sampled from two engine operating conditions—1200 rpm speed and 12 bar load as well as 2000 rpm speed and 6 bar load—are shown in Figures ~~S1 and S2~~S4–S7~~, respectively~~ below. The mass-mobility exponent of non-stripped particles was in the range of ~2.9–~3.0, which implies that these particles ~~were nearly spherical~~were primarily spherical semi-volatile particles. The mass-mobility exponent of stripped particles was in the range of 2.77–2.80, which indicates that the soot particles without any semi-volatile coating had a

compact structure. The discussion presented in the main manuscript about restructuring of non-volatile particles into compact clusters in the presence of a large amount of volatile material is also valid here. The compact structure of soot particles also manifests itself in effective density values that do not vary strongly with particle size.

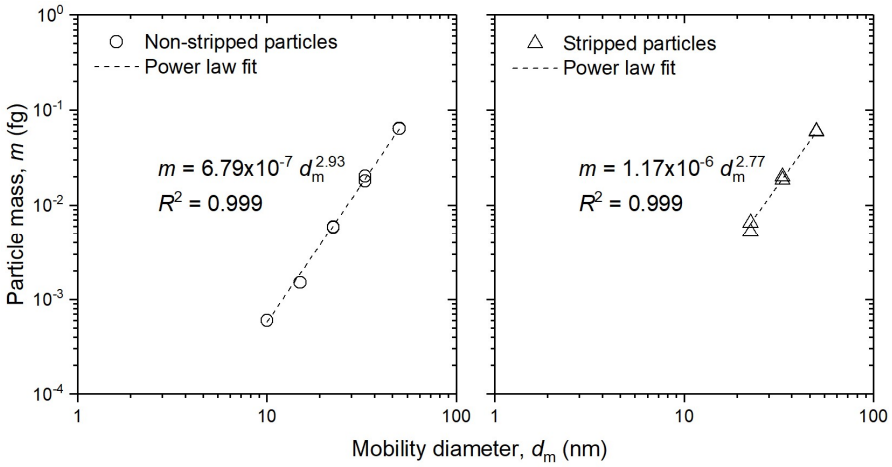

Figure S42: Representative mass-mobility relationship of non-stripped and stripped particles at engine speed of 1200 rpm and load of 12 bar using a DMA to select particles with certain mobility diameters and subsequently measuring their mass using a CPMA.

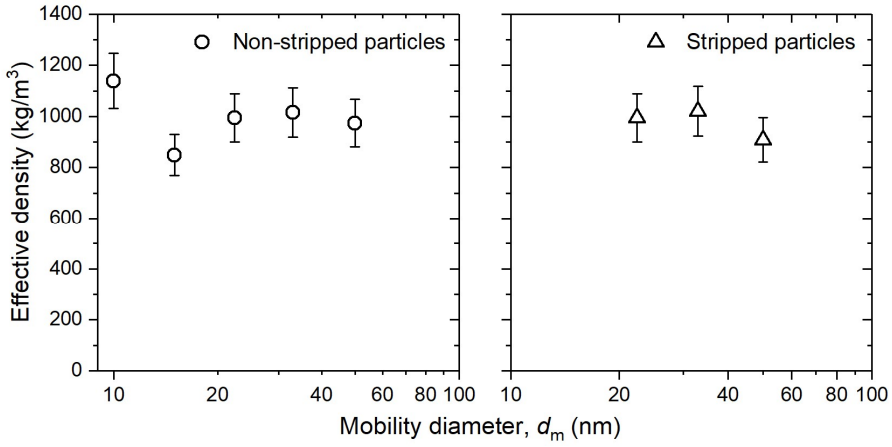

Figure S5: Representative effective density of non-stripped and stripped particles at engine speed of 1200 rpm and load of 12 bar using the DMA-CPMA tandem measurement.

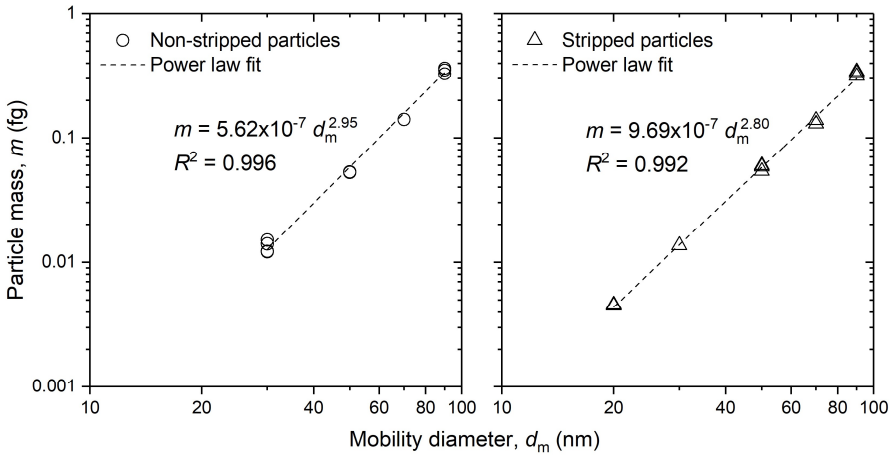

Figure S62: Representative mass-mobility relationship of non-stripped and stripped particles at engine speed of 2000 rpm and load of 6 bar using a DMA to select particles with certain mobility diameters and subsequently measuring their mass using a CPMA.

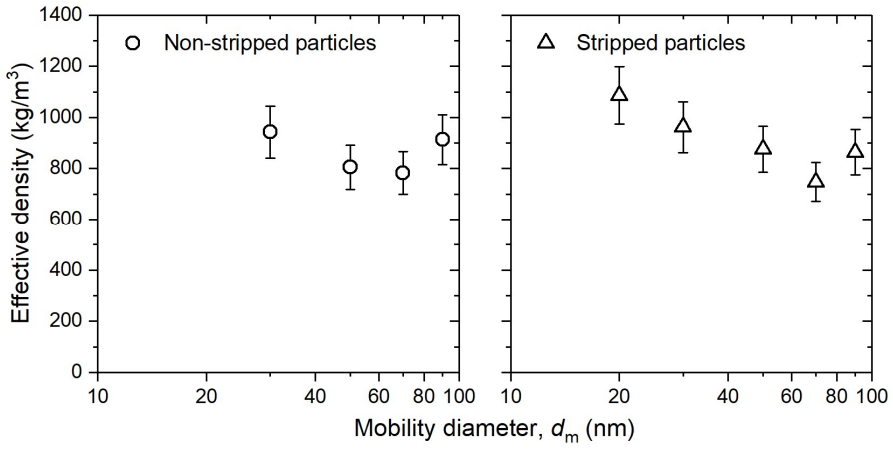

Figure S7: Representative effective density of non-stripped and stripped particles at engine speed of 2000 rpm and load of 6 bar using the DMA-CPMA tandem measurement.

References

Abernethy, R. B., Benedict, R. P., & Dowdell, R. B. (1985). ASME Measurement Uncertainty. *Journal of Fluids Engineering*, *107*(2), 161–164. https://doi.org/10.1115/1.3242450

Kim, J. H., Mulholland, G. W., Kukuck, S. R., & Pui, D. Y. H. (2005). Slip correction measurements of certified PSL nanoparticles using a nanometer differential mobility analyzer (Nano-DMA) for knudsen number from 0.5 to 83. *Journal of Research of the National Institute of Standards and Technology*, *110*(1), 31–54. https://doi.org/10.6028/jres.110.005

Kinney, P. D., Pui, D. Y. H., Mulholland, G. W., & Bryner, N. P. (1991). Use of the electrostatic classification method to size 0.1 micrometer SRM particles - A feasibility study. *Journal of Research of the National Institute of Standards and Technology*, *96*(2), 147. https://doi.org/10.6028/jres.096.006

Symonds, J. P. R., Reavell, K. S. J., & Olfert, J. S. (2013). The CPMA-electrometer system - A suspended particle mass concentration standard. *Aerosol Science and Technology*, *47*(8). https://doi.org/10.1080/02786826.2013.801547

Tavakoli, F., & Olfert, J. S. (2014). Determination of particle mass, effective density, mass-mobility exponent, and dynamic shape factor using an aerodynamic aerosol classifier and a differential mobility analyzer in tandem. *Journal of Aerosol Science*, *75*, 35–42. https://doi.org/10.1016/j.jaerosci.2014.04.010

Woo, M., Giannopoulos, G., Rahman, M. M., Swanson, J., Stettler, M. E. J., & Boies, A. M. (2021). Multiscale numerical modeling of solid particle penetration and hydrocarbons removal in a catalytic stripper. *Https://Doi.Org/10.1080/02786826.2021.1909700*, *55*(9), 987–1000. https://doi.org/10.1080/02786826.2021.1909700